Electronic Supplementary Material (ESI) for Nanoscale.


# Supplementary Information

# Dealloying-Based Facile Synthesis and Highly Catalytic Properties of Core/Porous Shell Nanoparticles

Minho Kim, Sung Min Ko, and Jwa-Min Nam*

Department of Chemistry, Seoul National University, Seoul 151-747, South Korea

* Correspondence to: jmnam@snu.ac.kr

# Experimental procedures

### Synthesis of Au-Ag alloy nanoparticles

We synthesized Au-Ag alloy nanoparticles based on the following literature procedures with a minor modification.[31] Typically, a solution containing 18.5 mL distilled water and 0.5 mM $AgNO_3$ aqueous solution was boiled at 100 $^oC$ for 10 min under magnetic stirring, 0.5 mM $HAuCl_4$ aqueous solution was then added to the mixture, and the resulting solution was boiled for 10 min. In this step, we adjusted the Au/Ag ratio of Au-Ag alloy nanoparticles by controlling the added volume of precursors (0.25 mL of $AgNO_3$ and 0.25 mL of $HAuCl_4$ solution for $Au_{50}Ag_{50}$ alloy nanoparticles; 0.375 mL of $AgNO_3$ and 0.125 mL of $HAuCl_4$ solution for $Au_{25}Ag_{75}$ alloy nanoparticles). Subsequently, freshly prepared 1 wt% trisodium citrate dihydrate solution (1 mL) was injected, and the resulting mixture was boiled for 30 min additionally. Finally, the solution was cooled to room temperature under ambient condition, and washed twice with distilled water by centrifugation at 7,000 rpm for 10 min.

### Dealloying reaction of Au-Ag alloy nanoparticles

Dealloying reaction was carried out by introducing $Fe(NO_3)_3$ solution and $HNO_3$ solution as a Ag etchant into the prepared Au-Ag alloy nanoparticles. In a typical synthesis, the Au-Ag alloy nanoparticle solution (250 μL) was mixed with 2 wt% PVP solution (250 μL), then 50 mM $Fe(NO_3)_3$ aqueous solution (25, 100, and 500 μL) or $HNO_3$ solution (60.0 %, 100 μL) was injected with gentle shaking. The resulting solution was mildly shaken for 30 min at room temperature, then washed twice with distilled water by centrifugation at 7,000 rpm for 10 min, and redispersed in distilled water.

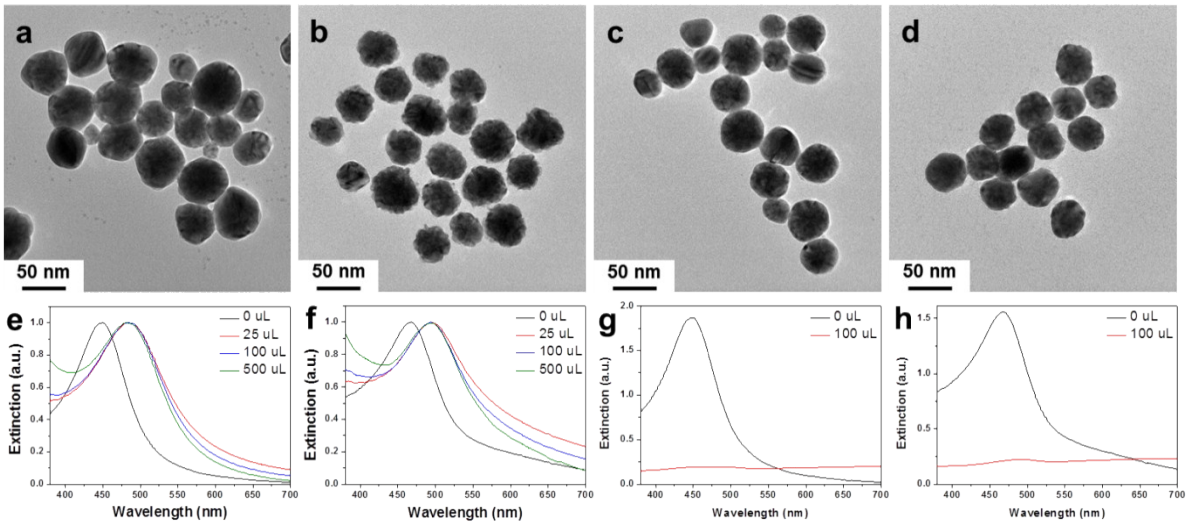


**Fig. S1.** The TEM images and UV-Vis spectra of Au-Ag alloy nanoparticles and their dealloyed structures. (a-d) TEM images of Au-Ag alloy and Au dealloyed nanoparticles: (a) $Au_{25}Ag_{75}$ alloy nanoparticles, (b) Dealloyed structures of $Au_{25}Ag_{75}$ alloy nanoparticles, (c) $Au_{50}Ag_{50}$ alloy nanoparticles, (d) Dealloyed structures of $Au_{50}Ag_{50}$ alloy nanoparticles. (e, f) The UV-Vis spectra of Au-Ag alloy nanoparticles and their corresponding dealloyed structures using $Fe(NO_3)_3$ as a Ag etchant: (e) $Au_{25}Ag_{75}$ alloy nanoparticles, (f) $Au_{50}Ag_{50}$ alloy nanoparticles. The single UV-Vis peak (black line) clearly demonstrates that as-synthesized nanoparticles composed of Au-Ag alloy nanoparticles only rather than a mixture of Au and Ag nanoparticles. As the added amount of Ag etchant [$Fe(NO_3)_3$] increased from 25 to 100 to 500 μL, the UV-Vis spectra were not shifted nor changed. (g, h) The UV-Vis spectra of Au-Ag alloy nanoparticles and their dealloyed structures using concentrated $HNO_3$ solution as a stronger Ag etchant: (g) $Au_{25}Ag_{75}$ alloy nanoparticles. (h) $Au_{50}Ag_{50}$ alloy nanoparticles. The UV-Vis peak disappeared after dealloying reaction, indicating collapse of nanostructures.

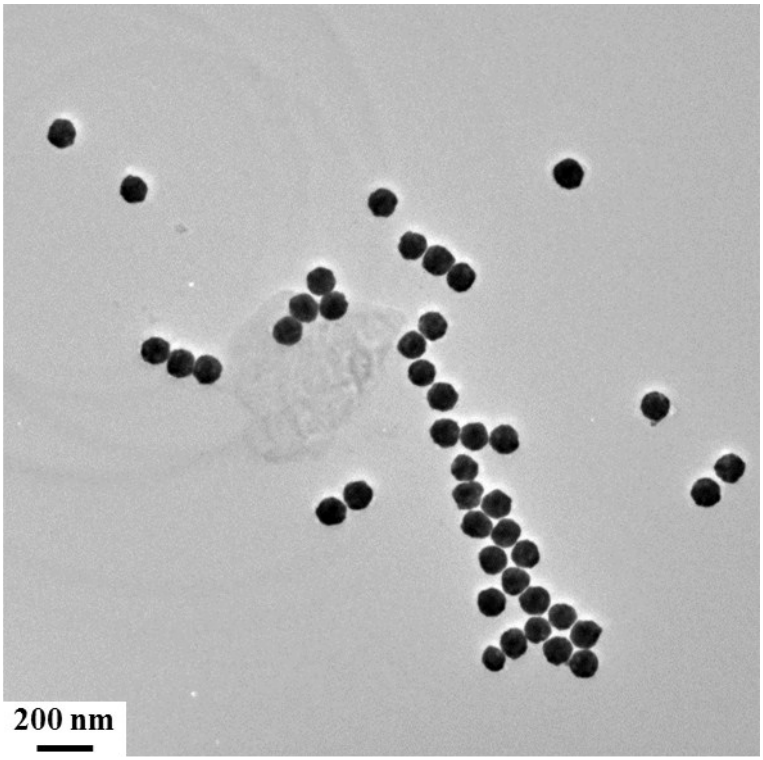


**Fig. S2.** The TEM image of CAS(7) NPs, showing a high-yield synthesis of the targeted structures.

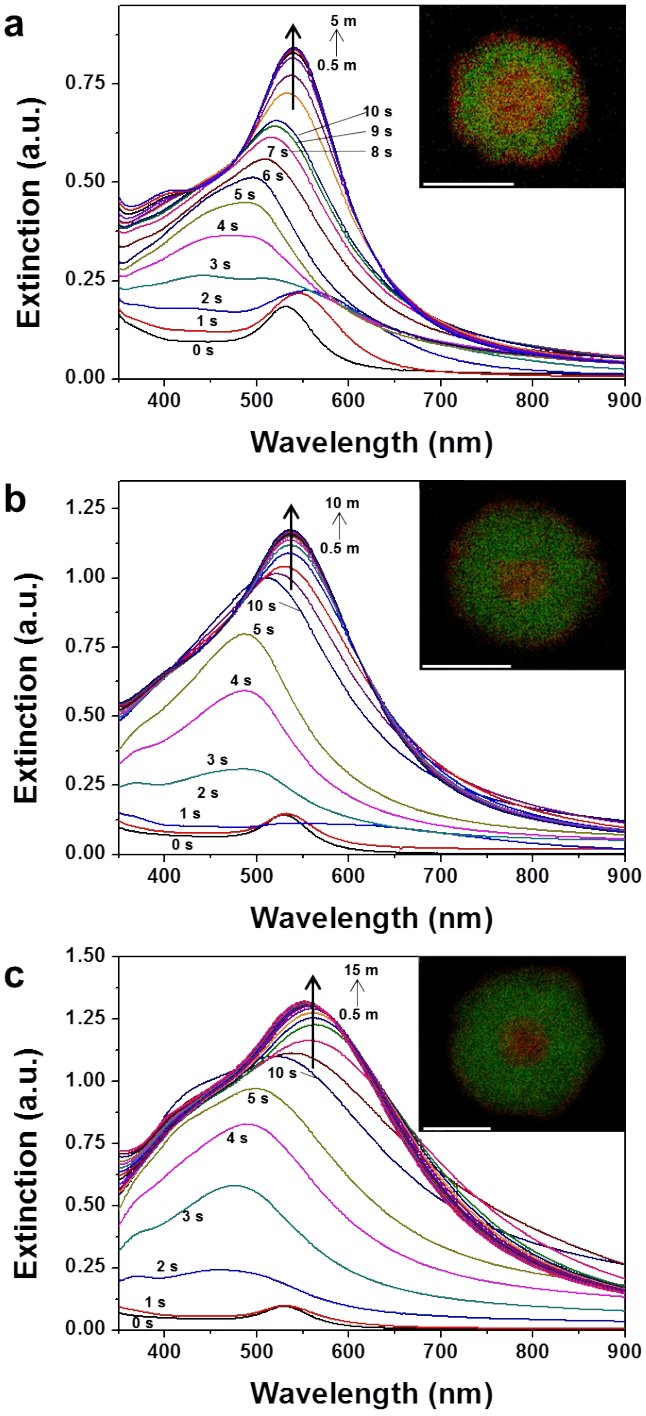


**Fig. S3.** The time-dependent UV-Vis spectral changes of the Au/Au-Ag core/alloy shell nanoparticles reaction mixture: (a) CAS(1) NPs, (b) CAS(3) NPs, (c) CAS(7) NPs. Insets represent corresponding EDX elemental mapping of CAS NPs. Scale bar = 50 nm.

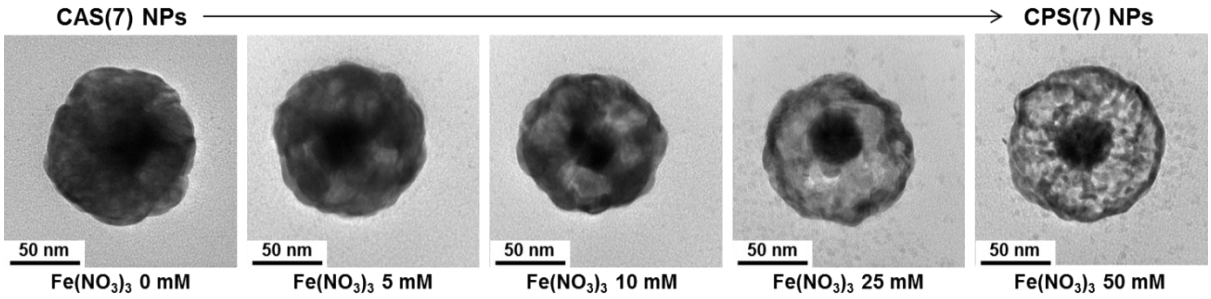


**Fig. S4.** The structural changes of CAS(7) NPs to CPS(7) NPs under dealloying reaction while increasing the amount of added $Fe(NO_3)_3$. Iron(III) nitrate acts as an Ag etchant (Ag(s) + $Fe(NO_3)_3$(aq) → $AgNO_3$(aq) + $Fe(NO_3)_2$(aq)). We propose a synthetic mechanism of CPS NPs as below. At the beginning of dealloying reaction, particles showed pinhole-like vacancies due to the dissolving Ag atoms in the Au-Ag alloy shell. As the reaction progressed, the number of dissolved Ag atoms increased, and Au and Ag atoms diffused outward during vacant areas diffused inward owing to the nanometer-scale Kirkendall effect. Because of difference in the diffusion rates of Au and Ag atoms in the Au-Ag alloy system (Ag atoms diffuse faster than Au atoms), the residual Ag atoms diffused outward and were continuously consumed by an Ag etchant. The Au atoms located in the alloy shell region diffused and were interconnected with each other to form thin ligaments [CPS(7) NPs].

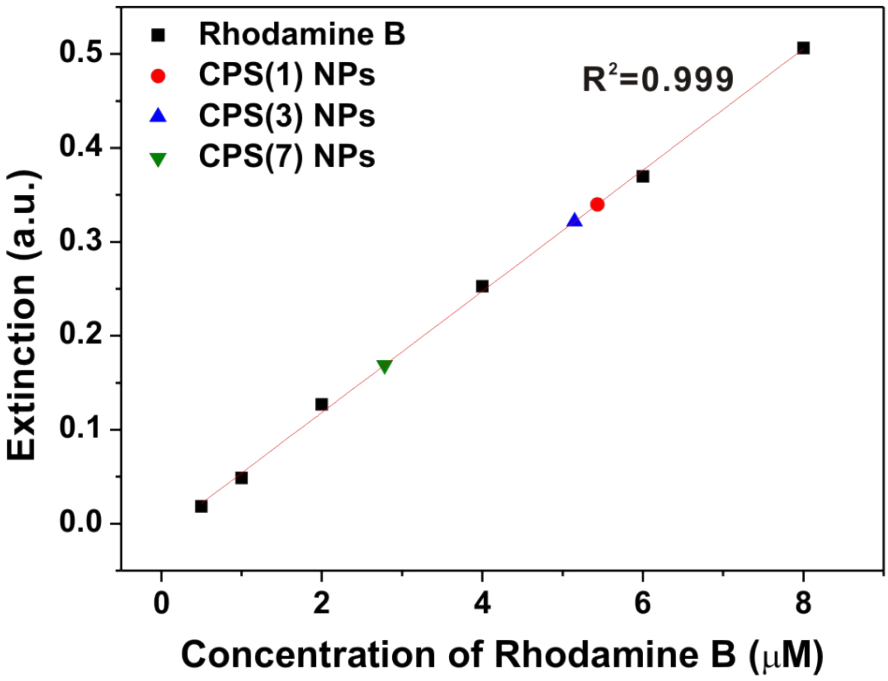


**Fig. S5.** The UV-Vis extinction standard curve of rhodamine B solution (black dots) for three CPS NPs. The UV-Vis extinction intensities of rhodamine B unattached after reaction with CPS NPs (red, blue, and green dots) were spotted on the standard curve. To obtain the concentration of unattached rhodamine B, first, the 225 pM CPS NP solution (200 μL) was mixed with 17.4 μM rhodamine B aqueous solution (100 μL), and the resulting solution was shaken for 2 hour at room temperature (the final concentration of CPS NPs and rhodamine B were 150 pM and 5.8 μM, respectively). Then, the UV-Vis extinction intensities of unattached rhodamine B (red, blue, and green dots) were measured from the supernatant of each mixture after centrifugation, and the concentration of unattached rhodamine B was calculated by fitting (the red line). From these results, the concentrations of rhodamine B loaded for each CPS NP were determined by subtracting from the initial concentration of rhodamine B (5.8 μM), and divided by the concentration of CPS NPs (150 pM) to obtain the loading capacity of each CPS NP. The data are summarized in Table S1.

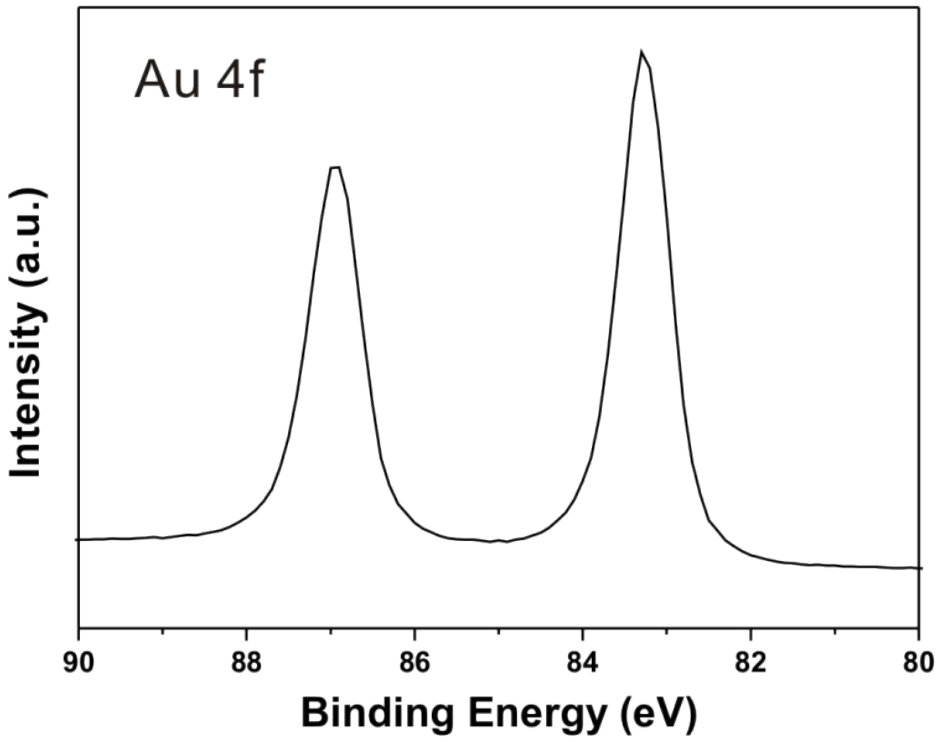


**Fig. S6.** The X-ray photoelectron spectroscopy (XPS) spectra of the CPS(7) NPs. The two peaks of Au 4f at 87.0 and 83.3 eV (separated by 3.7 eV) indicate the well reduced metallic Au surface.

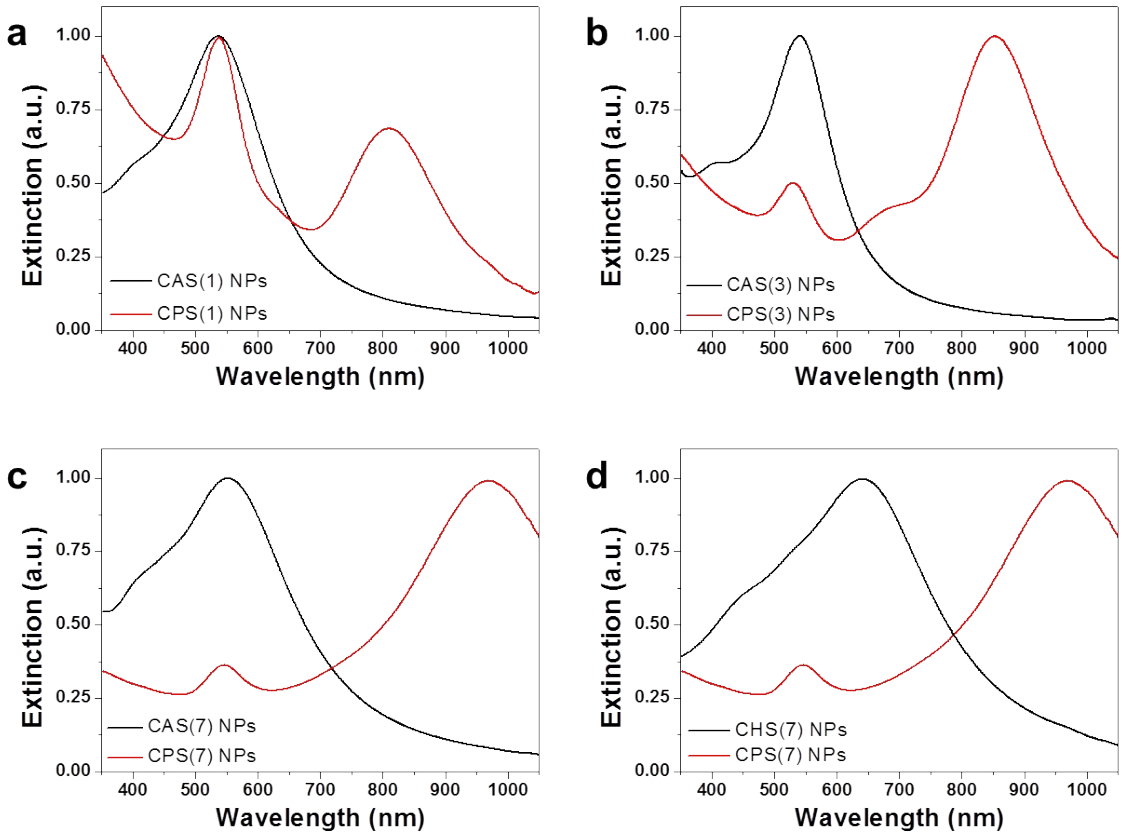


**Fig. S7.** The UV-Vis spectra of as-synthesized nanoparticles. (a-c) The UV-Vis spectra of Au/Au-Ag core/alloy shell nanoparticles (CAS NPs, black line) and the corresponding Au-based core/porous shell nanoparticles (CPS NPs, red line): (a) Ag/Au = 1, (b) Ag/Au = 3, (c) Ag/Au = 7. (d) The UV-Vis spectra of porous/hollow shell nanoparticles obtained by the galvanic replacement reaction (CHS(7) NPs, black line) and dealloying reaction (CPS(7) NPs, red line).

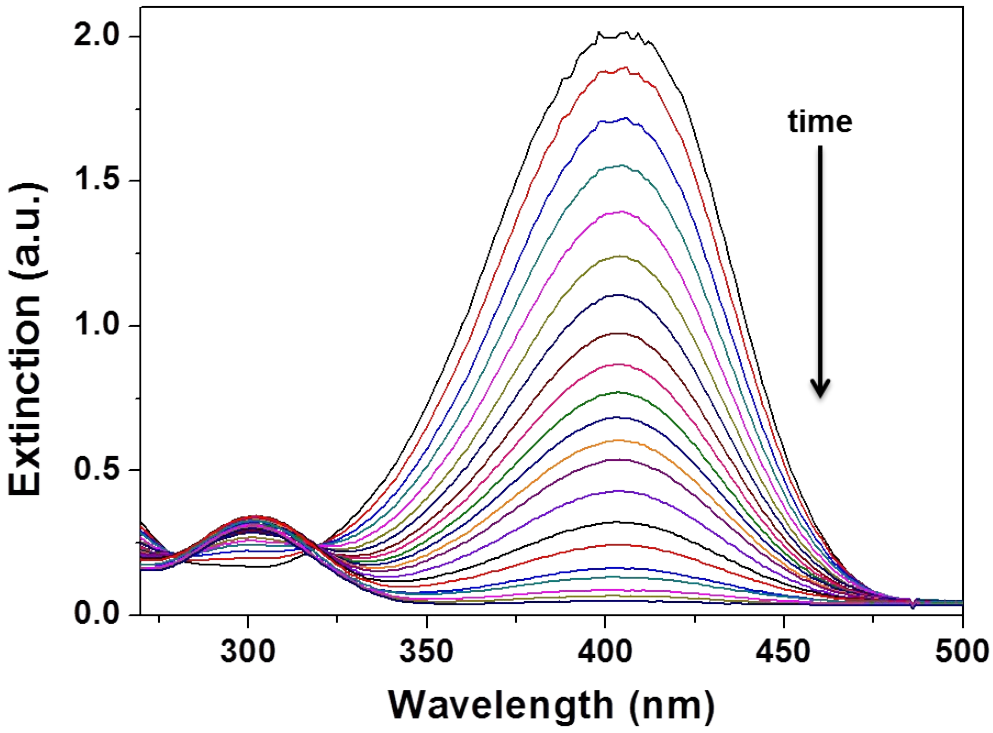


**Fig. S8.** The time-dependent UV-Vis spectral changes of 4-NP in the presence of nanocatalysts. The natural extinction peak of 4-NP is strongly exhibited at $\lambda$ = 317 nm, and shifts to $\lambda$ = 400 nm after freshly prepared $NaBH_4$ solution is added, indicating the formation of 4-nitrophenolate ions. However, it gradually decreases in the presence of a nanocatalyst with a new extinction peak arising at $\lambda$ = 300 nm, indicating conversion of 4-NP to 4-AP. During the successive decreases of the extinction peak at $\lambda$ = 400 nm, two isosbestic points are visible at $\lambda$ = 280 and 319 nm. These indicate that 4-NP was fully converted to 4-NP without side products in the catalytic reduction.

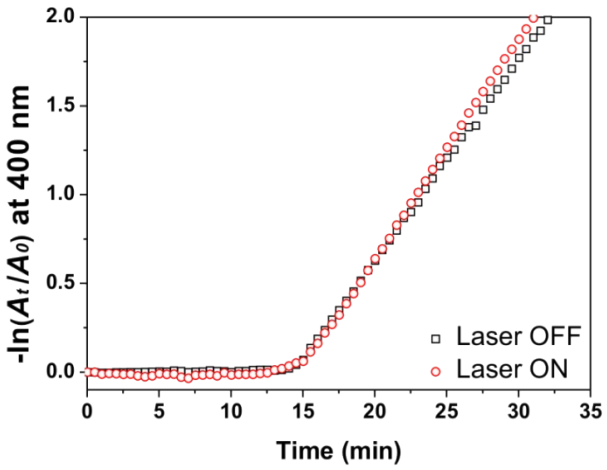


**Fig. S9.** The plots of -ln($A_t/A_0$) at $\lambda$ = 400 nm versus reaction time under the pseudo-first-order kinetics for CAS(7) NPs in the presence or absence of laser irradiation.

**Table S1.** The loaded amounts of rhodamine B per CPS NPs.

| | Initial concentration of rhodamine B (μM) | Concentration of unattached rhodamine B (μM) | Concentration of rhodamine B loaded on NPs (μM) | Loading capacity (number/particle) |
|---|---|---|---|---|
| CPS(1) NPs | 5.8 | 5.435 ± 0.013 | 0.365 ± 0.013 | 2434 ± 83 |
| CPS(3) NPs | 5.8 | 5.151 ± 0.015 | 0.649 ± 0.015 | 4326 ± 99 |
| CPS(7) NPs | 5.8 | 2.782 ± 0.015 | 3.018 ± 0.015 | 20119 ± 102 |

**Table S2.** The $k$ and $t_{ind}$ values for the catalytic reaction of CPS NPs and CHS(7) NPs performed at three different temperatures and that of CAS NPs and L-CHS(7) NPs† at 26.0 °C.

| | 13.5 °C | | 26.0 °C | | 44.0 °C | |
|---|---|---|---|---|---|---|
| | $k$ ($min^{-1}$) | $t_{ind}$ (min) | $k$ ($min^{-1}$) | $t_{ind}$ (min) | $k$ ($min^{-1}$) | $t_{ind}$ (min) |
| CPS(1) NPs | 0.121 ± 0.005 | 11.86 ± 0.02 | 0.219 ± 0.005 | 4.77 ± 0.07 | 0.548 ± 0.004 | 1.21 ± 0.02 |
| CAS(1) NPs | | | 0.202 ± 0.017 | 8.21 ± 0.59 | | |
| CPS(3) NPs | 0.204 ± 0.009 | 8.46 ± 0.01 | 0.343 ± 0.003 | 2.91 ± 0.03 | 0.742 ± 0.025 | 0.55 ± 0.03 |
| CAS(3) NPs | | | 0.138 ± 0.008 | 12.0 ± 0.75 | | |
| **CPS(7) NPs** | **0.483 ± 0.010** | **4.40 ± 0.01** | **0.708 ± 0.009** | **1.73 ± 0.01** | **1.261 ± 0.071** | **0.26 ± 0.03** |
| **L-CPS(7) NPs†** | | | **0.812 ± 0.014** | **1.11 ± 0.01** | | |
| CAS(7) NPs | | | 0.124 ± 0.011 | 13.8 ± 0.64 | | |
| CHS(7) NPs | 0.152 ± 0.014 | 6.62 ± 0.25 | 0.346 ± 0.014 | 2.28 ± 0.08 | 0.861 ± 0.030 | 0.59 ± 0.03 |

† The L-CPS(7) NPs (laser-irradiated CPS(7) NPs) were examined their catalytic performance at 26.0 °C under laser irradiation, of which the wavelength and power of laser source are 980 nm and 1.3 W, respectively.

**Table S3.** Summary of the activation energy ($E_a$), pre-exponential factor ($A$), and turnover frequency ($TOF_{50\%}$) values for nanocatalysts.

| | $E_a$ (kJ/mol) | $A$ ($min^{-1}$) | $TOF_{50\%}$ ($h^{-1}$) |
|---|---|---|---|
| CPS(1) NPs | 38.78 ± 1.46 | 7.6 – 23.3 (x $10^5$) | 182.0 ± 4.15 |
| CPS(3) NPs | 32.63 ± 1.68 | 8.8 – 33.8 (x $10^4$) | 285.0 ± 2.49 |
| **CPS(7) NPs** | **22.69 ± 1.35** | **3.8 – 11.3 (x $10^3$)** | **588.3 ± 7.48** |
| **L-CPS(7) NPs** | **-** | **-** | **674.8 ± 11.63** |
| CHS(7) NPs | 41.45 ± 1.96 | 2.7 – 12.5 (x $10^6$) | 287.5 ± 11.63 |

# Reference

31. S. Link, Z. L. Wang and M. A. El-Sayed, *J. Phys. Chem. B*, 1999, **103**, 3529-3533.